

Physics-constrained robust learning of open-form PDEs from limited and noisy data

Mengge Du^a, Longfeng Nie^b, Siyu Lou^{c,d}, Yuntian Chen^{c,e,*}, Dongxiao Zhang^{c,f,*}

^a*College of Engineering, Peking University, Beijing, 100871, P.R. China*

^b*School of Environmental Science and Engineering, Southern University of Science and Technology,
Shenzhen 518055, P. R. China*

^c*Eastern Institute for Advanced Study, Eastern Institute of Technology, Ningbo, 315200, Zhejiang, P.R.
China*

^d*Department of Computer Science and Engineering, Shanghai Jiao Tong University, 200240, Shanghai,
P.R.China*

^e*Ningbo Institute of Digital Twin, Eastern Institute of Technology, Ningbo, 315200, Zhejiang, P.R.
China*

^f*National Center for Applied Mathematics Shenzhen (NCAMS), Southern University of Science and
Technology, Shenzhen, 518000, Guangdong, P. R. China*

*Corresponding author

Email address: ychen@eias.ac.cn, zhangdx@sustech.edu.cn.

Abstract

Unveiling the underlying governing equations of nonlinear dynamic systems remains a significant challenge, especially when encountering noisy observations and no prior knowledge available. This study proposes R-DISCOVER, a framework designed to robustly uncover open-form partial differential equations (PDEs) from limited and noisy data. The framework operates through two alternating update processes: discovering and embedding. The discovering phase employs symbolic representation and a reinforcement learning (RL)-guided hybrid PDE generator to efficiently produce diverse open-form PDEs with tree structures. A neural network-based predictive model fits the system response and serves as the reward evaluator for the generated PDEs. PDEs with superior fits are utilized to iteratively optimize the generator via the RL method and the best-performing PDE is selected by a parameter-free stability metric. The embedding phase integrates the initially identified PDE from the discovering process as a physical constraint into the predictive model for robust training. The traversal of PDE trees automates the construction of the computational graph and the embedding process without human intervention. Numerical experiments demonstrate our framework's capability to uncover governing equations from nonlinear dynamic systems with limited and highly noisy data and outperform other physics-informed neural network-based discovery methods. This work opens new potential for exploring real-world systems with limited understanding.

Keywords: Symbolic representation; Hybrid PDE generator; Stability evaluation; Automatic PDE constraint embedding.

1. Introduction

For an extended period, the discovery of scientific knowledge has been largely obtained on the first principle. With the advancement of experimental science and the exponential increase in data, data-driven methods have attracted increasing attention. There is an urgent desire to efficiently extract physical knowledge from data, particularly governing equations, to enhance our understanding of the natural world.

Many linear and nonlinear dynamic systems are described by parsimonious PDEs. Consequently, this has led to the emergence of an important branch in the realm of knowledge discovery, namely, PDE discovery. The primary task of PDE discovery is to identify governing equations directly from data. The governing equations considered in most relevant studies can be represented as:

$$u_t = F(\Theta(u, x); \xi) \quad (1)$$

where u is the state variable of interest. The left-hand side (LHS) of the equation is a known function term represented by the time derivative of u . The target is to find an explicit nonlinear function F on the right-hand side (RHS) of the equation, which is composed of a library of function terms and their corresponding coefficients. Derived from the Sparse Identification of Nonlinear Dynamic Systems (SINDy) approach [1], PDE-find is a method that has brought about a significant breakthrough in the field of PDE discovery [2]. It proposes an algorithm named sequential threshold ridge regression to discover the linear combinations of function terms from measurements on a regular grid. Specifically, PDE-FIND signifies a static and predefined candidate library, consisting of monomial terms formed by u and its partial derivatives, which is shown below:

$$\Theta(u, x) = [1, u, \partial_x u, u(\partial_x u), u^2, (\partial_x^2 u), \dots, u^m (\partial_x^n u)] \quad (2)$$

where m and n represent the highest polynomial degree of u and the highest order of its partial derivatives, respectively. Eq (1) can then be transformed into

$$u_t = \Theta \xi = (1, u, \partial_x u, \dots, u^m (\partial_x^n u)) \cdot (\xi_1, \xi_2, \xi_3, \dots, \xi_{m \times n}) \quad (3)$$

where the majority of coefficients are relegated to zero to preserve the sparsity of the identified equation. Although PDE-find successfully uncovers many canonical dynamics systems, such as the Navier-Stokes equation and the reaction-diffusion equation, there are two significant limitations: (1) The construction of the library hinges heavily on strong assumptions and prior knowledge, which is not available and applicable to unknown systems. Consequently, a sufficiently large or overcomplete library is often required; (2) The method relies on numerical differentiation to assess partial derivatives on a regular grid, a practice that proves vulnerable to noise and sparse data, particularly in the context of high-order derivatives.

Given the limitations of the overcomplete library, subsequent studies have proposed methods based on an expandable library and even discovering open-form equations while preserving sparse regression. Essentially, the expandable library is capable of producing new equation terms through the interaction of predefined basis function terms. Based on the symbolic neural network proposed in EQL [3], PDE-Net 2.0 generates a flexible combination of operations and state variables by adjusting the network topology [4]. Compared with SINDy, it boasts a more compact library and the computational cost is significantly reduced. DLGA [5] and EPDE[6] integrated the genetic algorithm (GA) to substantially expand the original candidate set through the recombination of gene fragments (via mutation and crossover operations). Nevertheless, the expressive power of the

interactive space remains limited. Only multiplication and addition operations are introduced in the generation of interactive function terms, which is insufficient to discover open-form equations. Actually, in the early studies, many researchers tried to uncover analytical relations from nonlinear dynamic systems through symbolic mathematics [7,8]. SGA further combined symbolic representations and GA and represented PDEs with different function terms of tree structure [9]. This method greatly increases representation flexibility, but the introduction of crossover and mutation operations may lead to poor iterative stability of the generated equations. To counter this, the following research named DISCOVER further utilized the neural-guided agent to generate PDEs and accelerate the optimization process with deep reinforcement learning (RL) [10]. Note that symbolic mathematics enables the discovery of open-form PDEs, thus circumventing the high-memory consumption and computational requirements of overcomplete library methods.

Some research has concentrated on tackling the second problem from various perspectives, such as employing the weak-formulation method [11–13] or Bayesian estimation [14–17] to deal with noisy and limited data. A significant branch of this research field is based on the neural networks-based method. Specifically, these algorithms tended to utilize deep neural networks to approximate the noisy system response, thereby allowing for the seamless evaluation of derivatives through automatic differentiation [18–20]. With the development of physics-informed neural network (PINN) [21,22], some methods tried to incorporate the loss term of physics into the neural network training process to enhance the robustness to noisy observations. A framework named DeepMod marks a significant breakthrough, which put forward a fully differentiable method for revealing the underlying governing equations with the training paradigm of PINN [23]. In this framework, a new loss term, composed of the residuals between the linear combinations of library terms and the time derivative (i.e., LHS) is integrated into the training process. The coefficients of function terms are kept sparse by the constraint of L_1 regularization and the final function terms are ascertained via a hard threshold. Similar to this method, PINN-SR employed sparse regression to evaluate the coefficients and executed STRidge along with the training of the neural networks using an alternating direction optimization strategy (ADO) strategy [24]. In subsequent studies, the methods have been further refined; for instance, PDE_READ substituted the regular fully connected network with two rational neural networks [25], and Thanasutives et al. incorporated the discrete Fourier transform (DFT) in a multi-task learning paradigm for data denoising [26]. Although methods combined with PINN augment the ability to extract correct equations from noisy data, it is apparent that these methods rely on a predefined compact library based on prior knowledge. Otherwise, the computational inefficiency of embedding all of the function terms into the physics loss is unbearable. A sufficiently large library poses more challenges in identifying the parsimonious equation. Fine-tuning the hyperparameters of sparsity for different systems and noise levels proves unreasonable and impractical.

In this paper, we propose a framework named R-DISCOVER, which is aimed at simultaneously solving the two problems present in PDE-find based on prior work of DISCOVER [10]. We utilize symbolic representations to represent PDEs instead of a pre-defined basis function library to uncover open-form PDEs. A neural network (NN) is used to predict state variables, and the equations discovered are embedded as physical constraints to handle limited and sparse data. Particularly, the process of identifying the underlying equations via the proposed R-DISCOVER comprises two primary procedures: the discovery process and the embedding process. The discovering process combines a RL-guided hybrid PDE generator and a NN-based reward

evaluator (also a predictive model) to discover better-fitting PDEs. During the embedding process, the initially identified PDEs obtained from the discovering process are automatically incorporated as a physics loss into the NN to enhance its robustness to noisy data with a PINN-training paradigm. The alternating training of these two processes completes the closed loop of knowledge discovery and embedding, with the primary objective of uncovering underlying equations from limited and noisy data.

The main contributions of this framework are mainly as follows:

- It seamlessly integrates symbolic mathematics and automatic equation embedding to robustly discover open-form PDEs from limited and noisy data.
- A RL-guided hybrid PDE generator is designed to generate diverse PDE expressions with a tree structure. It combines RL, GA, and a dynamic subtree bank to deal with complex equations even including multiple state and spatial variables in lengthy form. Mathematical and physical constraints, such as spatial symmetry, are considered to reduce the search space.
- We incorporate bootstrapped data to conduct stability evaluation, striking a balance between data fitness and stability of coefficients. The proposed metric is parameter-free and exhibits robustness across different scenarios.
- The numerical experiments demonstrate that our framework can correctly uncover governing equations from linear and nonlinear dynamic systems even when faced with highly noisy and limited data. Its robustness and accuracy surpass other related PINN-based discovery methods.

The structure of this paper is organized as follows: We elucidate the specific operations of the framework, focusing on equation discovery in Section 2.1 and automatic PDE constraint embedding in Section 2.2. In Section 3, we demonstrate the framework's capability to reveal governing equations under conditions of limited and noisy data through six numerical experiments and provide a comparative analysis with related methods. Lastly, in the conclusion, we present our primary findings and discuss potential avenues for future research.

2. Methodology

The framework aims to leverage symbolic representation to find free combinations of symbols including u , spatial-temporal variables x and t , i.e., we believe the form of $\Theta(u, x)$ is as follows:

$$\Theta(u, x) = [f_1(u, x), f_2(u, x), \dots, f_n(u, x)] \quad (4)$$

This kind of representation liberates the constraints of a fixed candidate library and enables the discovery of more complex equation structures, such as fractional (u/x) and compound structures ($\partial_x^2(u^2)$). Assuming that the accessible noisy and sparse measurements can be denoted

as $U_m = \{\tilde{u}(t_j, x_j)\}_{j=1}^{N_m} \subseteq (0, T] \times \Omega$, and sampled collocation points are represented as $U_c = \{\hat{u}(t_i, x_i)\}_{i=1}^{N_c} \subseteq (0, T] \times \Omega$, our goal is to directly extract the explicit form of the governing equations from them.

2.1 Overview of the proposed framework

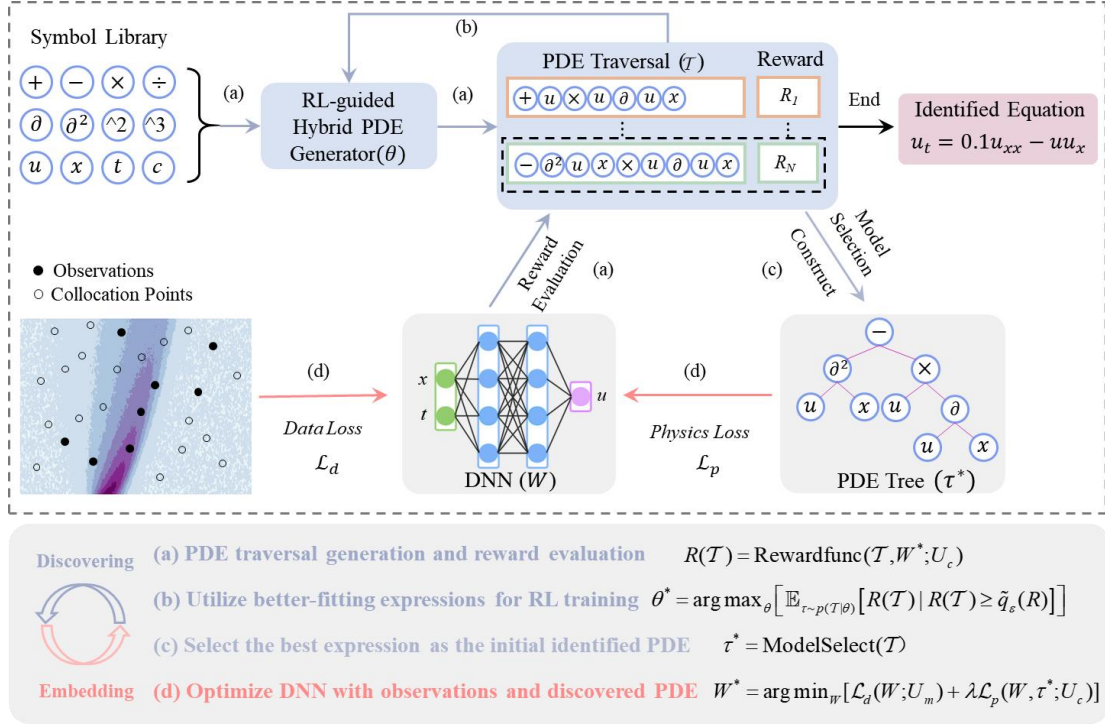


Fig. 1 Overview of R-DISCOVER for discovering Burgers' equation from limited and noisy data.

To effectively mine correct governing equations from limited and noisy data, we propose the R-DISCOVER framework as illustrated in Fig. 1. The workflow of our proposed framework consists of two primary steps: discovering and embedding. During the discovering process, our objectives- corresponding to (a), (b), and (c) in Fig. 1, are to generate and explore as many high-reward PDE representations as possible that best match the current data information. We first preset a symbol library and utilize an RL-guided hybrid PDE generator to generate PDE expressions. It utilizes an enhanced LSTM agent proposed in DISCOVER [10] to batch-generate initial samples. Then those samples are filtered as the initial population for GA and an adjustable module named dynamic subtree bank for generating expressions with more diverse representation. These expressions are represented in the form of PDE traversal, specifically, pre-order traversal of the corresponding tree structure. Subsequently, we evaluate the reward through a NN-based prediction network (predicting system response). The LSTM agent is updated by the risk-seeking policy gradient method with selected better-fitting expressions to provide a better initial population. Finally, we perform model selection based on the refined PDE candidates, thoroughly evaluating data fitness and the stability of coefficients. The optimal PDE is then chosen as the initially identified PDE for subsequent physics embedding in DNN. The second step corresponds to the embedding process, as depicted in Fig. 1 (d), where the physical constraints are automatically embedded into the computational graph by traversing the PDE tree to calculate the residuals. Combined with supervised learning of observations, the prediction network can be trained and optimized in a similar manner to PINN. The main purpose of step 2 is to utilize the preliminary identified equations as physical constraints so that they can evaluate the rewards in the discovering stage more accurately, and enhance the robustness to noise. Overall, these two steps

are complementary processes, with the former mining underlying physical information from the data, and the latter applying PDE constraints to better correct the data information in the mining process. The strategy of alternating iterative updates like ADO [24] is implemented to obtain the final accurate and concise governing equation.

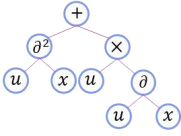
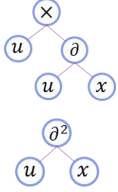
2.2 Discovering process

In this section, we will provide a detailed description of the discovery process, including the representation, generation, evaluation, optimization, and selection of the PDE.

2.2.1 Symbolic representations for open-form PDEs

To uncover the open-form governing equation underlying the nonlinear dynamic systems, we adopt a symbolic representation to express the equation. First, we need to define a symbol library consisting of two categories of symbols, i.e., operators ($\{+, -, \times, \div, \partial, \partial^2, \wedge^2, \dots, \text{etc}\}$) and operands ($\{u, x, t, \dots, \text{etc}\}$). For example, if we consider the RHS of Burgers' equation, which is $u_{xx} + uu_x$, it can be represented in several related forms as shown in Table 1. A PDE can be represented by a binary tree structure, where the non-leaf nodes are operators and the leaf nodes are operands. A binary operator needs two operands to satisfy the requirement of full degree, such as $+$. For a unary operator, it requires only one operand. Based on these syntactic relationships, a PDE tree and its pre-order traversal are in one-to-one correspondence. Furthermore, the PDE tree can be further partitioned into smaller-level representations, i.e., function terms or subtrees, according to the $+$ and \times operators on the top of trees. It's worth noting that to simplify the process, we do not consider the coefficients of the equation terms during the generation process. These coefficients can be evaluated during the reward evaluation phase.

Table 1 Illustration of different forms of PDE and its compositions.

Mathematical expression	PDE expressions		Function terms	Subtree
	PDE Traversal	PDE tree		
$u_{xx} + uu_x$	$\{+\partial^2ux \times u\partial ux\}$		$\{u_{xx}, uu_x\},$ $\{\partial^2ux, u\partial ux\}$	

2.2.2 Hybrid PDE traversal generator (RL/GA/DSB)

Next, we provide a more detailed explanation of the PDE generation process. Given the complexity of generating a PDE expression tree, the previous work DISCOVER, employed a neural-based sequence generator to efficiently batch-generate corresponding PDE pre-order traversals [10]. Specifically, an enhanced structure-aware LSTM serves as the agent. By leveraging structured input in conjunction with monotonic attention, the agent effectively captures structured information, making it suitable for handling PDE traversal sequences with inherent

structural attributes. Note that while the neural-based generator can accelerate the search process based on historical high-quality samples, it is also prone to falling into local optima. At the same time, compared to an overcomplete library, free combinations of symbols result in a larger search space, which significantly increases the training burden. To address these issues, our framework proposes a hybrid PDE generator by further integrating genetic operations from GA and dynamic subtree bank to generate diverse equation representations. The hybrid generation can leverage the advantages of each method, reducing the number of iterations while being more conducive to the discovery of complex and lengthy governing equations. As shown in Fig. 2 (a), the generated PDE traversals consist of three parts:

- **RL set:** The PDE samples from the RL set are batch-generated by the neural-based agent (parameterized by θ) in a step-by-step manner. Particularly, at i^{th} iteration, the token τ_i is sampled from the symbol library on the probability distribution of probability distribution $p(\tau_i | \tau_{1:(i-1)}; \theta)$ emitted by the LSTM agent. The likelihood of a complete pre-order traversal can then be represented by $p(\tau | \theta) = \prod_{i=1}^{|\tau|} p(\tau_i | \tau_{1:(i-1)}; \theta)$. Physical and mathematical constraints are also embedded by modifying the library distribution to reduce the search space and ensure the generation of reasonable expressions. For example, the left child node following a partial differential operator (\hat{c}) cannot be a spatial variable (such as x). More details can be found in [10].
- **GA set:** The initial population of the GA set is derived from high-quality samples in the RL set with higher rewards. As illustrated in Fig. 2 ①, through the crossover and mutation operations in GA, new offspring are produced and constitute the GA set. Crossover operates on function terms, while mutation targets tree nodes, i.e., operands or operators. This process mainly mimics the transmission and expression of genes in a population, increasing the diversity of equation representations. It's worth noting that in each iteration of GA, the initial population undergoes a restart operation based on the samples generated by RL, which is a more favorable approach compared to random initialization.
- **Expressions from dynamic subtree bank:** The dynamic subtree bank (DSB) is constructed based on samples generated from both RL and GA. First, we select high-quality samples and split each sample into function terms. Then, frequent terms are selected from the pool of function terms to form the DSB. Common sparse regression is then utilized to generate new PDE expressions with the optimization objective $\hat{\xi} = \arg \min_{\xi} \|\Theta \xi - u_i\|_2^2 + \lambda \|\xi\|_0$, as shown in Fig. 2 ②. What's different is that the l_0 penalty is not a fixed value, but dynamically adjusted according to the mean squared error (MSE) of the RHS and LHS of the best PDE expression up to the current iteration. It can be expressed by $\lambda = \delta \text{MSE}(\Theta^* \xi^*, u_i)$ where i refers to the current iteration and δ is randomly sampled from a preset interval, such as $\delta \in [0.1, 0.5]$, allowing for the generation of PDE expressions with different levels of sparsity penalty. At the same time, the function term library is also subsampled from the DSB to further increase the diversity of generation.

The RL-guided hybrid PDE generator essentially leverages a learnable agent to generate a good initial population, expands the combinations among the high-quality expressions through GA,

and then confluences the high-quality genes through a dynamic subtree bank. The whole generation process is outlined in Algorithm 1.

Algorithm 1 Generation of PDE expressions by RL-guided hybrid PDE generator

- 1: **Input:** LSTM agent with parameter θ ; Size of initial population N ; Size of dynamic subtree bank N_f ; Size of subsampled basis function library N_{sub} ; Basis function library split from the best expression Θ^* .
 - 2: $T_{RL} \leftarrow \{\tau_i \sim p(\cdot | \theta)\}_N^{i=1}$ // Initiate PDE traversals with a LSTM agent.
 - 3: $T_m \leftarrow Mutation(T_{RL})$ // Generate N traversals through mutation
 - 4: $T_c \leftarrow Crossover(T_{RL})$ // Generate 2N traversals through crossover
 - 5: $T_{GA} = T_m \cup T_c$ // Merge the expressions generated by GA.
 - 6: $T = T_{RL} \cup T_{GA} = \{\tau_i\}_N^{i=1}$ // Filter and keep best N expressions.
 - 7: Select frequent function terms from T to form a dynamic subtree bank.

$$\Psi = \{\psi_i\}_{i=1}^{N_f}$$
 - 8: **For** i in $1, 2, \dots, N$ **do**
 - 9: $\phi \equiv Random(0.1, 0.5)$ // randomly generate a coefficient for sparse penalty
 - 10: $\Theta_i = \text{subsample}(\Psi) = \{\psi_i\}_{i=1}^{N_{sub}}$ // Subsample DSB and form basis function library.
 - 11: $\lambda = \phi MSE(\Theta^* \xi^*, u_i)$
 - 12: $\hat{\xi} = \arg \min_{\xi} \|\Theta_i \xi - u_i\|_2^2 + \lambda \|\xi\|_0$
 - 13: Select function terms with large coefficients to form PDE traversal and add it to candidate set:

$$T_{DSB} \leftarrow \tau_i \leftarrow \{\psi_j : |\hat{\xi}_j| > tol, j \in 1, 2, \dots, N_{sub}\}$$
 - 14: **End**
 - 15: **Output:** PDE expressions for training $T_{train} = T \cup T_{DSB}$
-

Common sparse regression can be employed to lessen the complexity of searching for equation representations in discrete space. Note that for multidimensional nonlinear systems, there often exist multiple spatial derivatives, such as $\{\omega_x, \omega_y, \omega_{xx}, \omega_{yy}\}$ in Navier-Stokes (NS) equations, which typically exhibit symmetrical relationships in spatial dimensions, i.e., the number of occurrences of x and y should be consistent. However, it is challenging for the PDE expressions to obey this constraint in the generation stage. To solve this, our algorithm further introduces a spatial correction to ensure the symmetry properties of physics. For example, the PDE expressions generated by the above method may appear as irregular cases such as $u\omega_x + v\omega_y + \omega_{xx}$. By

introducing two correction methods of addition and deletion, we can transform it into $u\omega_x + v\omega_y$ and $u\omega_x + v\omega_y + \omega_{xx} + \omega_{yy}$, making it more physically meaningful and avoiding the generation of invalid forms. The hybrid generator, complemented by spatial symmetry constraints, enables our framework to have the ability to deal with complex governing equations from nonlinear dynamic systems even with multiple variables.

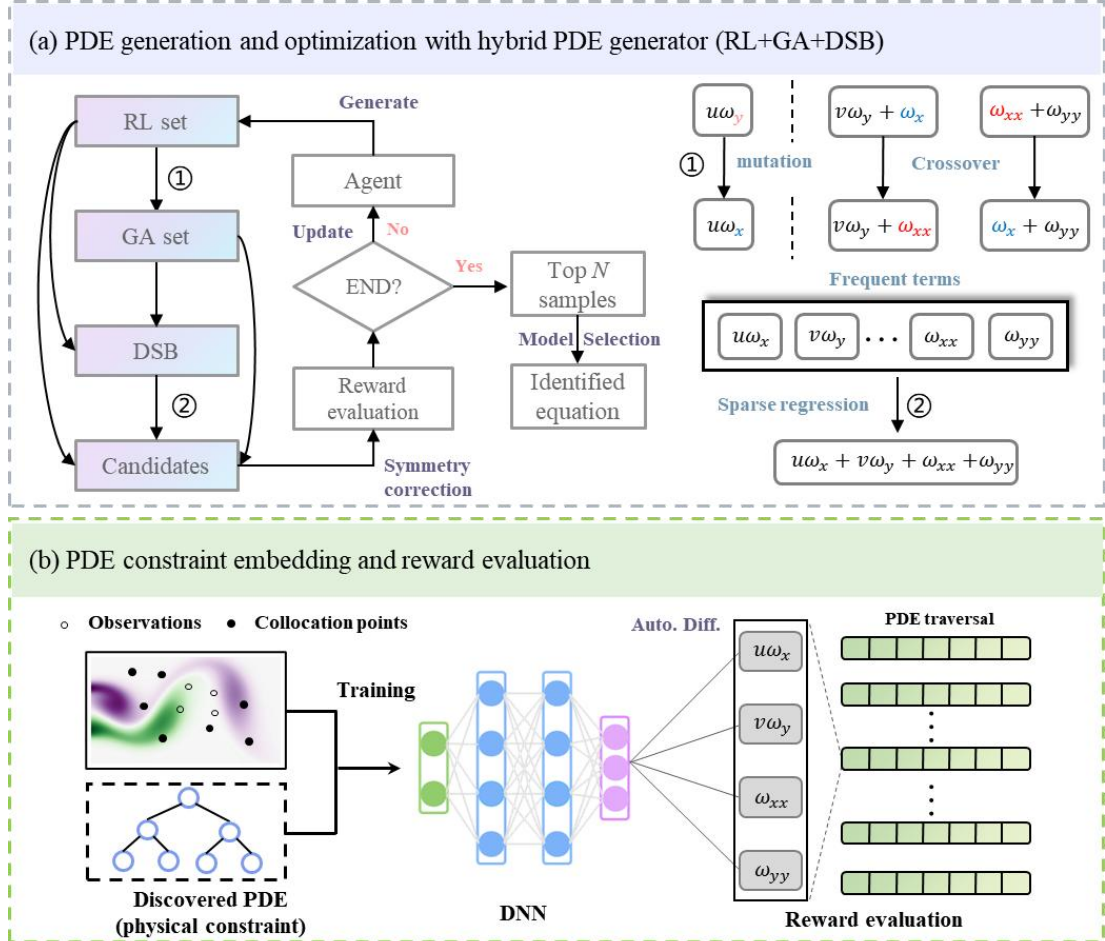


Fig. 2 Illustration of the identification of Navier-Stokes equation. (a) PDE generation and optimization with RL-guided PDE generator; and (b) PDE constraint embedding and reward evaluation.

2.2.3 Reward evaluation

After generating PDE expressions, it's necessary to further evaluate their rewards. Here, we first need to split the PDE expressions into function terms according to '+' or '-' on the top of trees. Then, based on Sequential Threshold Ridge regression (STRidge) [2], we determine the coefficients of function terms as follows:

$$\hat{\xi} = \arg \min_{\xi} \left| \Theta(u, x) \xi - u_t \right|_2^2 + \kappa \|\xi\|_2^2 \quad (5)$$

when $\kappa=0$, the regularization term becomes ineffective and this method reduces to the Sequentially Thresholded Least Squares method (STLS). With the function terms and their coefficients determined, a complete PDE representation can be obtained. We then evaluate the rewards of the generated PDE expressions with following metrics:

$$R(\tau) = \frac{1 - \zeta_1 \times d_{max} - \zeta_2 \times n}{1 + RMSE}, RMSE = \sqrt{\frac{1}{N_c} \sum_{i=1}^{N_d} (\Theta(u_i, x_i) \xi - u_i)^2} \quad (6)$$

where d_{max} represents the maximum depth of the subtree structure corresponding to the function terms, and n denotes the number of function terms. The former is used to measure the complexity of a single equation term, while the latter is used to measure the complexity of the PDE traversal τ . ζ_1 and ζ_2 represent the penalties for the above two complexities, used to ensure the simplicity of the equation form. The RMSE in the numerator is used to measure the fitness of observations. Here, we first utilize the predictive model to fit the state variable u , and then utilize automatic differentiation to evaluate the partial derivatives, which is robust to noise. The concrete process is illustrated in Fig. 2 (b).

2.2.4 Optimization with the risk-seeking policy-gradient method

In this problem, since the parameters of the agent cannot be updated directly by the reward function using gradient descent, the reinforcement-learning strategy is utilized. In detail, we adopt the risk-seeking policy gradient method, which is dedicated to improving the performance of the better-fitting expressions in the generated samples [27,28]. This is mainly because our task aims to uncover the best-performing equation representation rather than to maximize the expectation of all of the rewards. We need to sort the rewards of all samples and select $(1 - \varepsilon)$ -quantile reward $\tilde{q}_\varepsilon(R)$ as a threshold. Samples with rewards higher than $\tilde{q}_\varepsilon(R)$ can be utilized as training samples. The goal of optimization can be represented as

$$J_{\text{risk}}(\theta; \varepsilon) \doteq \mathbb{E}_{\tau \sim p(\tau|\theta)} [R(\tau) | R(\tau) \geq R_\varepsilon(\theta)] \quad (7)$$

Its gradient can be calculated using the following equation.

$$\nabla_\theta J_{\text{risk}}(\theta; \varepsilon) \approx \frac{\lambda_{pg}}{\varepsilon N_{train}} \sum_{i=1}^{N_{train}} [R(\tau^{(i)}) - \tilde{q}_\varepsilon(R)] \cdot \mathbf{1}_{R(\tau^{(i)}) \geq \tilde{q}_\varepsilon(R)} \nabla_\theta \log p(\tau^{(i)} | \theta) \quad (8)$$

where N refers to all of the PDE expressions generated from the hybrid generator at each iteration; λ_{pg} refers to a hyperparameter that measures the importance of the risk-seeking policy-gradient method; and $\mathbf{1}_x$ denotes a conditional judgment that returns 1 when the condition represented by x is true and 0 otherwise.

2.2.5 Model selection by considering the stability of coefficients

Through iterative optimization, the hybrid generator produces and accumulates some high-quality PDE samples. We perform a preliminary evaluation of them through the reward function and select the top K PDE candidates for the model selection. The evaluation is further refined from the perspective of coefficients stability. In related studies, the statistical performance of coefficients on a subset of full data has also been taken into consideration like E-SINDy [29]

and other methods based on the moving horizon technique [30,31]. In this paper, we propose a comprehensive evaluation metric to comprehensively assess the accuracy and stability of discovered PDEs. The best PDEs are selected through majority voting, as shown in Fig. 3.

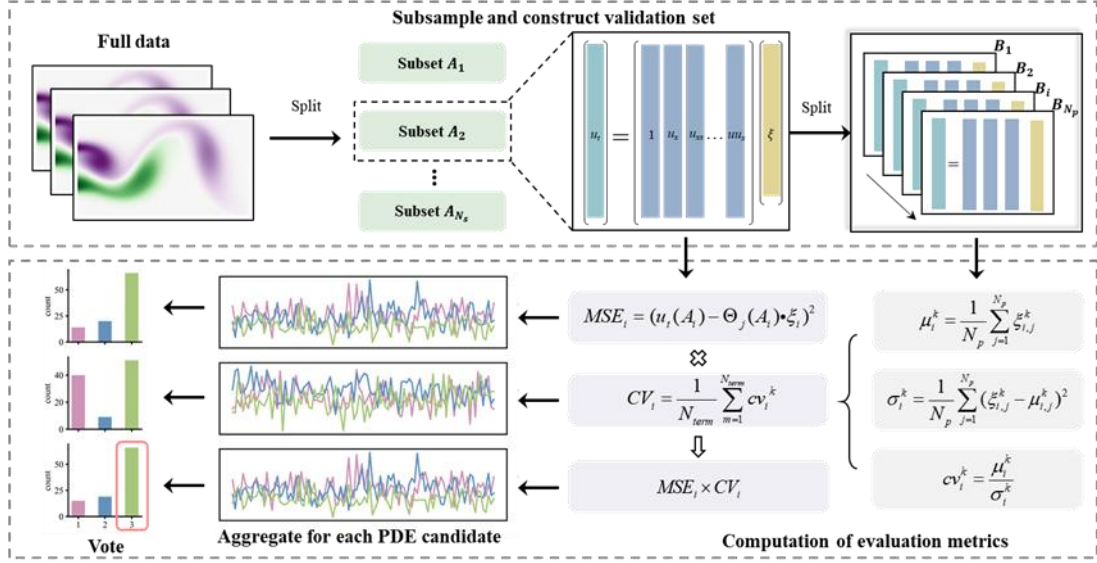


Fig. 3 Schematic of model selection based on data fitting and coefficients stability.

The primary idea is that distinguishing between necessary and redundant terms through a single fit on the full dataset is challenging. However, it is expected that essential function terms will consistently possess non-zero coefficients when a series of fits are conducted on various sub-sampled datasets. In contrast, the redundant terms, which primarily serve as fitting for noise, are likely to have a drastic change of coefficients on each subsample. Taking one of the PDE candidates with function library as an example, we first utilize randomly sampled collocation points and DNN to generate the dataset $U_c = \{\hat{u}(t_i, x_i)\}_{i=1}^{N_c} \subseteq (0, T] \times \Omega$, and N_s bootstrapped subsets are sampled with equal size of $N_c / 2$. The coefficients of each PDE candidates are then calculated based on regular least squares method and we further evaluate the MSE between the LHS and the RHS of the PDE as a measure of the accuracy of data fitting. It is represented by

$$MSE_i = (u_i(A_i) - \Theta(A_i) \cdot \xi_i)^2, i = 1, 2, \dots, N_p \quad (9)$$

Where A_i refers to the subset of full data. Then, subsets are further split into subsamples $B_j \subset \{1, 2, \dots, N_c / 2\}$, $j = 1, 2, \dots, N_p$ of equal size $N_c / 4$. For each subsample in subset A_i , the coefficients are recalculated and the coefficients of variation (cv) for term k can be obtained by

$$cv_i^k = \frac{\mu_i^k}{\sigma_i^k} \quad (10)$$

where μ_i^k and σ_i^k refer to the mean and standard deviation of the k^{th} term of current PDE candidate in subset A_i , respectively. And for the PDE candidate, it can be further evaluated by

$$CV_i = \frac{1}{N_{term}} \sum_{k=1}^{N_{term}} cv_i^k \quad (11)$$

We can use the product of the MSE and CV as a measure of the performance of each PDE candidate on each subset. Finally, we aggregate and rank these measures and take a majority vote to select the best PDE. The detailed procedures are illustrated in Fig. 3.

2.3 Physics embedding process

The practice of embedding physics, especially governing equations, into neural networks named physics-informed neural network has been widely studied and discussed [21,32]. It has been proved to be an effective way to improve the prediction accuracy and robustness to noise. In this section, we will demonstrate how R-DISCOVER embed discovered equations into neural networks as physical constraint automatically by means of structural properties of the PDE tree. Without halting the training midway, the framework achieves a complete and complementary closed-loop process of knowledge discovery and embedding.

2.3.1 Automatic physics embedding with identified PDEs incorporated

There are two aspects of loss that need to be considered when training a predictive model: data loss and physics loss. They can be represented as follows:

$$L_d(W) = \frac{1}{N_m} \sum_{i=1}^{N_m} |\hat{u}_i - NN_W(x_i, t_i)|^2 \quad (12)$$

$$L_p(W) = \frac{1}{N_c} \sum_{i=1}^{N_c} |R(W, \tau^*; U_c)|^2 = \frac{1}{N_c} \sum_{i=1}^{N_c} |u_t(x_i, t_i) - \Theta(u_t, x_i) \bullet \xi|^2 \quad (13)$$

where W represents the trainable parameters in DNN and τ^* is the initially identified PDE obtained by model selection. The coefficients of PDE are set to be trainable at the last iteration.

According to Eq., the key to imposing physical constraints is to solve for the residuals on the RHS and LHS of initially identified PDE. However, the exact form of PDEs cannot be predetermined at each iteration, and which means we cannot explicitly write them into the program as is typically done with common PINN does. In this paper, we adopt an approach from the automatic machine learning, specifically an automatic knowledge embedding framework named AutoKE [33], which automatically construct computational graphs by means of traverse PDE trees. We first reconstruct the PDE traversal obtained from the discovering process into a PDE tree. Since all of the operations are performed using operators from deep learning frameworks, such as Pytorch [34], the computational graph can be constructed automatically during the traversal of PDE tree to calculate the residual. Partial derivatives can be evaluated by the automatic differentiation in the neural network, as shown in Fig. 2 (b).

Besides, we also incorporate an optional smoothing trick in the training process. Since the noisy data may increase the bias of the network prediction, a local sampling strategy is utilized. We resample some collocation points around the observations and create a new loss term by

$$L_l(W) = \frac{1}{N_l} \sum_{i=1}^{N_l} |u_t(x_i, t_i) - \Theta(u_t, x_i) \bullet \xi|^2 \quad (14)$$

Where N_l is the number of collocation points resampled around observations. Consequently, the total PINN loss can be represented as

$$L(W) = L_d + \lambda_1 L_p + \lambda_2 L_l \quad (15)$$

Where λ_1 and λ_2 represent the hyperparameters for measuring the importance of corresponding loss terms. The default value of the latter λ_2 is 0, However, according to experience, when encountering highly noisy and sparse observations, this loss term can have a significant corrective effect on the prediction.

In the training process, automatically embedding the mined physical information into the neural network effectively enhances the robustness of prediction to noise. This improvement is beneficial for predicting the state variable and evaluating partial derivatives in the discovery process.

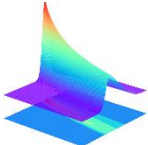
3 Results

3.1 Data descriptions and evaluation metrics

In this section, we verify the framework's ability to identify governing equations of six nonlinear dynamic systems in the presence of limited and highly noisy data. These six equations mainly include classical Burgers' equation, Fisher–Kolmogorov–Petrovsky–Piskunov (Fisher–KPP) equation and nonlinear Fisher-KPP equations with a square of the spatial derivative, the Kuramoto–Sivashinsky (KS) equation with high-order spatial derivatives, Navier-Stokes equations with multiple state variables and 3D Gray–Scott reaction-diffusion model with 2 PDEs included and only low-resolution data available. The descriptions of these six equations are shown in Table 2.

The total training process includes three parts, pretraining with the observations, discovering open-form PDEs, and embedding PDE constraints into the DNN. The latter two are alternately updated as illustrated in the Section 2. In the experiments, to minimize the training time as possible, we carry out only two rounds of the alternating iteration process. During the pretraining parts, we divide the observations into training set and validation set with at a ratio of 8:2. We use the Adam optimizer to fit the noisy data and determine the end of training based on the performance of the validation set. During the discovering process with symbolic representation, only the top 10% of expressions are selected to update the agent. More detailed descriptions about the hyperparameters are provided in supplementary material.

Table 2 Descriptions of canonical dynamic systems utilized in this paper.

Equation		Descriptions
Burgers' equation		$x \in [-8, 8]_{n_x=256}, t \in [0, 10]_{n_t=101}$, Sample ratio 3.19%~19.34% Noise level (σ): 10%~125%
$u_t = -uu_x + 0.1u_{xx}$		

Fisher-KPP equation		$x \in (-1, 1)_{nx=199}, t \in (0, 1)_{nt=99}$ Sample ratio: 10%~25% Noise level (σ): 10%~100%
Nonlinear Fisher-KPP		$x \in (-1, 1)_{nx=199}, t \in (0, 1)_{nt=99}$ Sample ratio 25%~50% Noise level (σ): 10%~50%
Kuramoto-Sivashinsky (KS)		$x \in [-10, 10]_{nx=512}, t \in [0, 50]_{nt=256}$, Sample ratio: 5%~50% Noise level (σ): 10%~30%
Navier-Stokes equation (NS)		$x \in [0, 6.5]_{nx=325}, y \in [0, 3.4]_{ny=170}$, $t \in [0, 30]_{nt=150}$ Sample ratio: 0.72% Noise level (σ): 5%~25%
3D Gray-Scott reaction-diffusion model		$x \in [-1.25, 1.25]_{nx=32}, y \in [-1.25, 1.25]_{ny=32}$, $z \in [-1.25, 1.25]_{nz=32}, t \in [0, 10]_{nt=100}$ Sample ratio: 10 % Noise level (σ): 0~10%

We use four metrics to evaluate the ability of the proposed framework to identify governing equations. The first one is the relative error of the coefficients, which is used to measure the difference between the uncovered coefficients and the true coefficients, as follows

$$E = \frac{1}{N} \sum_{i=1}^N \frac{|\xi_i^* - \xi_i|}{|\xi_i|} \times 100\% \quad (16)$$

where N denotes the number of function terms; ξ_i^* and ξ_i represent the estimated and true values of the i^{th} term, respectively. This metric can only be applied when the discovered function terms align with the true equations. In addition, we introduce two other metrics, relative coefficient error E2 and the true positive rate (TPR), to measure the performance when the mined equations are not exactly correct. They are evaluated by

$$E_2 = \frac{\|\xi^* - \xi\|_2}{\|\xi\|_2}, \quad TPR = \frac{TP}{TP + FN + FP} \quad (17)$$

True positive (TP) denotes the count of non-zero coefficients in ξ that have been accurately identified while false negative (FN) refers to the number of coefficients in ξ that are incorrectly identified as zero. On the other hand, false positive (FP) corresponds to the number of coefficients in ξ that are mistakenly identified as non-zero. Higher values of true positive rate (TPR) indicate

that the actual equation form has been approximated more accurately, and a TPR value of 1 signifies that the correct equation form has been successfully retrieved.

Given the spatio-temporal information, the neural network trained in this framework can be used to further predict the physical field of state variables of interest, which is the advantage of combining prediction network (DNN) and PINN compared with other numerical discovery methods, like SINDy. Therefore, another evaluation metric l_2 error is utilized to measure the relative error between the reconstructed physical field and the real physical field.

$$L_2(u_{pred}, u_{true}) = \frac{\|u_{pred} - u_{true}\|_2}{\|u_{true}\|_2} \quad (18)$$

We added gaussian noise to the observations to verify the robustness of the framework. The way of applying the noise is shown below

$$u(x, t) = u(x, t) + \sigma \cdot std(u) \cdot N(0, 1) \quad (19)$$

3.2 Experiments

3.2.1 Discovering Burgers' equation

The Burgers' equation utilized here is a prototypical example of a nonlinear partial differential equation, which exhibits a wide range of complex phenomena, including shock waves, rarefaction waves, and turbulence [33,34]. We provide the performance for discovering it under different noise and data amounts. As shown in Fig. 4, the coefficients of the discovered equations diverge from true values as the noise level increases and the data quantity decreases. This divergence continues until incorrect function terms are mined or certain true function terms are omitted. When the correct equation terms are identified, the physical constraints can help improve the accuracy of the physical field derived from the reconstruction. Conversely, it can also increase the error. With more than 2000 data points (about 8% of the total data points), the current framework can successfully mine the correct equations even in the presence of up to 125% white noise.

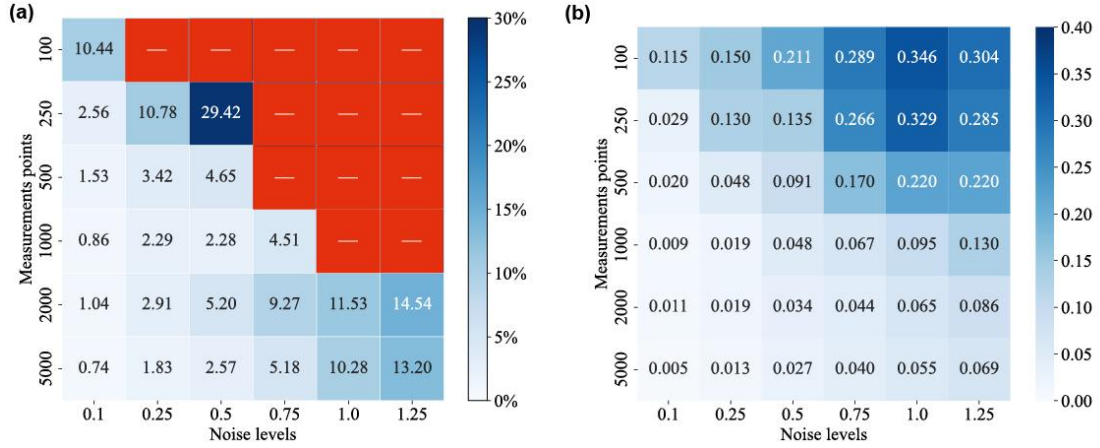


Fig. 4 Mean of relative coefficient E (a) and the relative full-field l2 error (b) under different fractions of data and white noise. The red square indicates that the discovered equation terms are not consistent with the ground truth.

Fig. 5 further illustrates the optimization process in the presence of a data volume of 5000 and 100% noise. The robustness of the prediction results can be enhanced by constraining the output of the DNN with the discovered equations after each alternate iteration of the process, leading to a notable increase in reward. The final identified equation is as follows:

$$u_t = -0.958uu_x + 0.0836u_{xx} \quad (20)$$

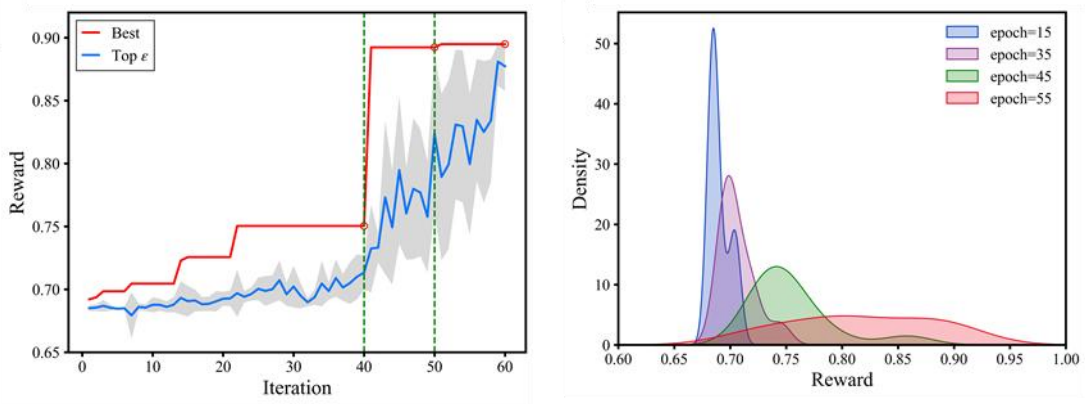


Fig. 5. (Left): the evolution of the best reward and top ϵ fraction of rewards for 5000 data points (20% of the total data points) with 100% gaussian noise. The positions marked by the green dashed line and the red hollow circle indicates the start of each new round of the search process after the DNN is updated. (b) The Gaussian kernel density estimate of the top fraction of rewards.

Fig. 6 demonstrates the predicted results by DNN when the discovered PDE constraint is incorporated. It can be seen that the predicted results are consistent with the exact solution except for some errors at the boundary.

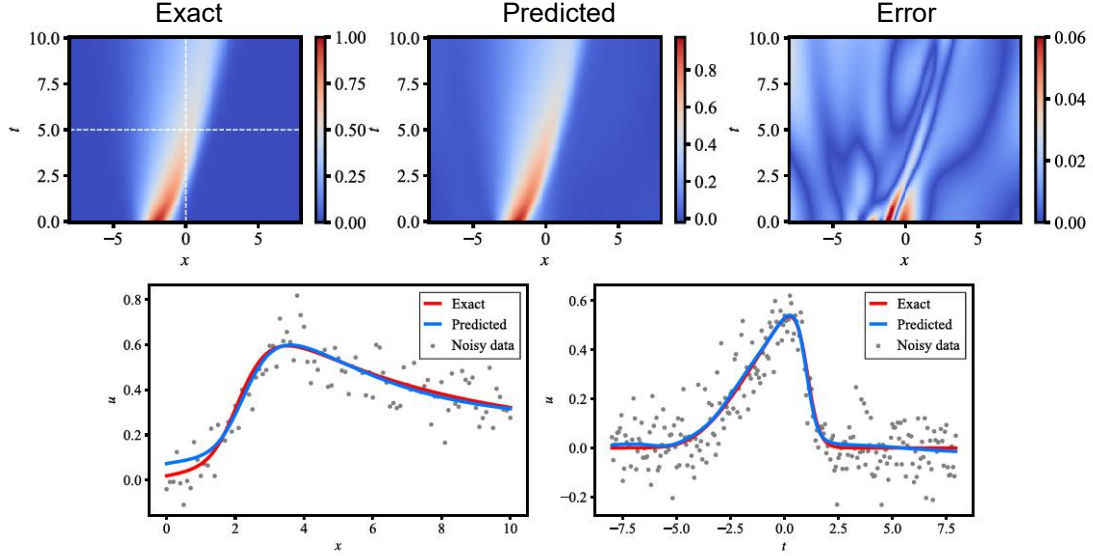


Fig. 6. The comparison between the true and predicted solution. The white dashed line refers to the location of the line plot below.

3.2.2 Discovering biological transport model described by Fisher-Kolmogorov-Petrovsky-Piskunov (Fisher-KPP) equations

The Fisher-KPP equation is a simplified version of the reaction-diffusion equation. The equation has been the subject of extensive study in the fields of mathematical biology and is used to model a wide range of physical systems, including combustion [35], epidemics [36], and tumor growth [37]. In this experiment, we consider both classical and nonlinear Fisher-KPP forms, where the latter equation has a more complex form especially including a square of the spatial derivative ($(u_x)^2$), which are not taken into consideration in most overcomplete library methods. In the absence of a priori knowledge, assuming that the governing equations are composed of monomials of u and its partial derivatives with the form of $u^m (\partial_x^n u)^k$. The number of total possible terms can be represented with $N_l(m, n, k) = (m+1)(n*k+1)$, which grows dramatically when large orders are considered. For example, $N_l(3, 3, 2) = 28$ and $N_l(5, 5, 3) = 96$. This can greatly increase the DNN training time and computational burden, especially in high-dimensional dynamic systems with multiple state and spatial variables.

Table 3 Discovery of classical Fisher-KPP equation for 5000 data points under different levels of noise.

Correct PDE: $u_t = 0.02u_{xx} + 10u - 10u^2$			
Noise level	Identified PDE	E (%)	L_2 error
25%	$u_t = 0.02u_{xx} + 9.735u - 9.68u^2$	2.78	0.017
50%	$u_t = 0.022u_{xx} + 9.54u - 9.675u^2$	5.95	0.026
75%	$u_t = 0.021u_{xx} + 9.314u - 9.118u^2$	7.23	0.039
100%	$u_t = 0.021u_{xx} + 9.314u - 9.118u^2$	10.80	0.046

Table 4 Discovery of nonlinear Fisher-KPP equation for 5000 data points under different levels of noise.

Correct PDE: $u_t = 0.02uu_{xx} + 0.02u_x^2 + 10u - 10u^2$			
Noise level	Identified PDE	E (%)	L_2 error
10%	$u_t = 0.019uu_{xx} + 0.019u_x^2 + 9.994u - 10.011u^2$	2.04	0.006
25%	$u_t = 0.014uu_{xx} + 0.014u_x^2 + 9.988u - 9.963u^2$	14.62	0.010
50%	$u_t = 0.011uu_{xx} + 0.011u_x^2 + 9.840u - 9.896u^2$	22.2	0.016

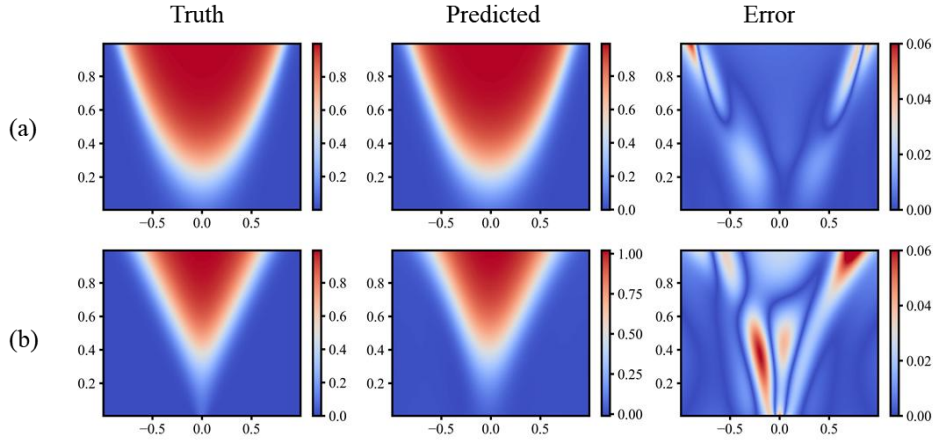


Fig. 7 Predicted solutions of (a) classical; (b) nonlinear Fisher-KPP equations. The results are obtained under 100% noise and 50% noise, respectively.

Since our framework only considers the function term of the optimal expression when embedding PDEs, it can effectively alleviate this problem. When mining classical Fisher-KPP, our framework can correctly identify the correct equation terms with at most 100% noise as shown in Table 3 with 5000 data points available. For the Non-linear Fisher-KPP equation, due to the stronger nonlinearity of the system, the evaluation of the equation terms will be more complicated and challenging. When uncovering this equation, with 10,000 observations, it can resist at most 50% of the noise, and the error of its equation coefficients is relatively larger compared to the classical one. The details are demonstrated in Table 4. The predicted solutions of those two equations with maximum noise are presented in Fig. 7

3.2.3 Discovering Kuramoto–Sivashinsky equation

The KS equation utilized here describes the evolution of a one-dimensional fluid flow in the presence of nonlinearity, dispersion, and diffusion. The term uu_x represents the advection term, the term u_{xx} represents the diffusion term, and the term u_{xxxx} represents the fourth-order dispersion term. Compared to other equations, higher-order derivatives increase the difficulty of discovery of the equation under noisy data. To cope with this approach, we introduce the weak-form method in the evaluation of the equation terms, which can reduce the order of the derivatives and improve the accuracy of the derivative evaluation. We take the collocation points uniformly in the defined

computational region $x \in [-6, 6]$ and $t \in [10, 40]$, where 1200 points and 300 points are uniformly taken in the space and time direction respectively. In the design of DNN, we use $\sin(x)$ as the activation function, and the fully connected network is set to 3 layers with 128 neurons in each layer, which is aimed at reducing the error caused by calculating the derivatives with the chain rule.

Table 5 Discovery of KS equation for 26215 data points (20% of total) with different levels of noise.

Correct PDE: $u_t = -uu_x - u_{xx} - u_{xxx}$			
Noise level	Identified PDE	Error (%)	L_2 error
5%	$u_t = -0.996uu_x - 0.989u_{xx} - 0.988u_{xxx}$	1.01	0.009
10%	$u_t = -0.982uu_x - 0.984u_{xx} - 0.988u_{xxx}$	1.14	0.016
20%	$u_t = -0.960uu_x - 0.942u_{xx} - 0.938u_{xxx}$	4.95	0.020
30%	$u_t = -0.941uu_x - 0.885u_{xx} - 0.879u_{xxx}$	9.46	0.029

In this case, we tested the robustness of the framework with different data volumes and noise. As shown in Table 5, the correct equations can be identified with only 20% of the data from the original simulation points are used when up to 30% noise is added. More detailed results about the sensitivity of data volume are shown in Table 6. This example demonstrates that our framework can effectively identify the governing equations of complex dynamic systems with high-order derivatives.

Table 6 Discovery of KS equation with 15% noise and different volumes of data.

Correct PDE: $u_t = -uu_x - u_{xx} - u_{xxx}$			
Data Volume	Identified PDE	Error(%)	L_2 error
$N = 52429$ (40%)	$u_t = -0.988uu_x - 0.986u_{xx} - 0.988u_{xxx}$	0.90	0.013
$N = 39322$ (30%)	$u_t = -0.982uu_x - 0.984u_{xx} - 0.988u_{xxx}$	1.15	0.016
$N = 26214$ (20%)	$u_t = -0.975uu_x - 0.954u_{xx} - 0.953u_{xxx}$	3.55	0.016
$N = 13108$ (10%)	$u_t = -0.978uu_x - 0.953u_{xx} - 0.948u_{xxx}$	3.65	0.021
$N = 6554$ (5%)	$u_t = -0.931uu_x - 0.896u_{xx} - 0.903u_{xxx}$	8.64	0.032

3.2.4 Discovering Navier-Stokes equation (NS)

The Navier-Stokes equations are widely used in computational fluid dynamics to analyze and predict the behavior of fluids in various situations [38,39]. Notably, the introduction of the multiple state variable (ω, u, v) and two-dimensional space (x, y) increases the number of basic operators. It significantly increases the number of possible combinations of symbols, which in turn expands the search space and increases the difficulty of discovering the correct equation. On the other hand, the correct equation contains four terms with different derivatives, which further increases the challenge of using a sequence model to generate the equation representation. As shown in Fig. 7, under the condition of 25% noise, we compare the RL generator (only the LSTM agent utilized) with the hybrid generator in discovering the equations. It can be found that the common RL method is unable to find the correct combination of equations in a shorter period, and tends to be trapped in a local optimal. The wrong equations will further mislead the training of DNN. For the hybrid generator, it is possible to collect the possible function terms by fully utilizing the compact subtree library, and based on the correction of the symmetry of the space, the correct equations can be found in a shorter iteration step.

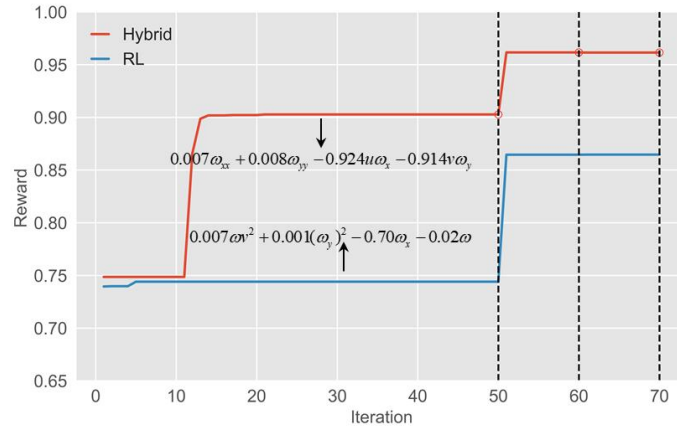


Fig. 8. The evolution of the best reward with RL generator and hybrid generator.

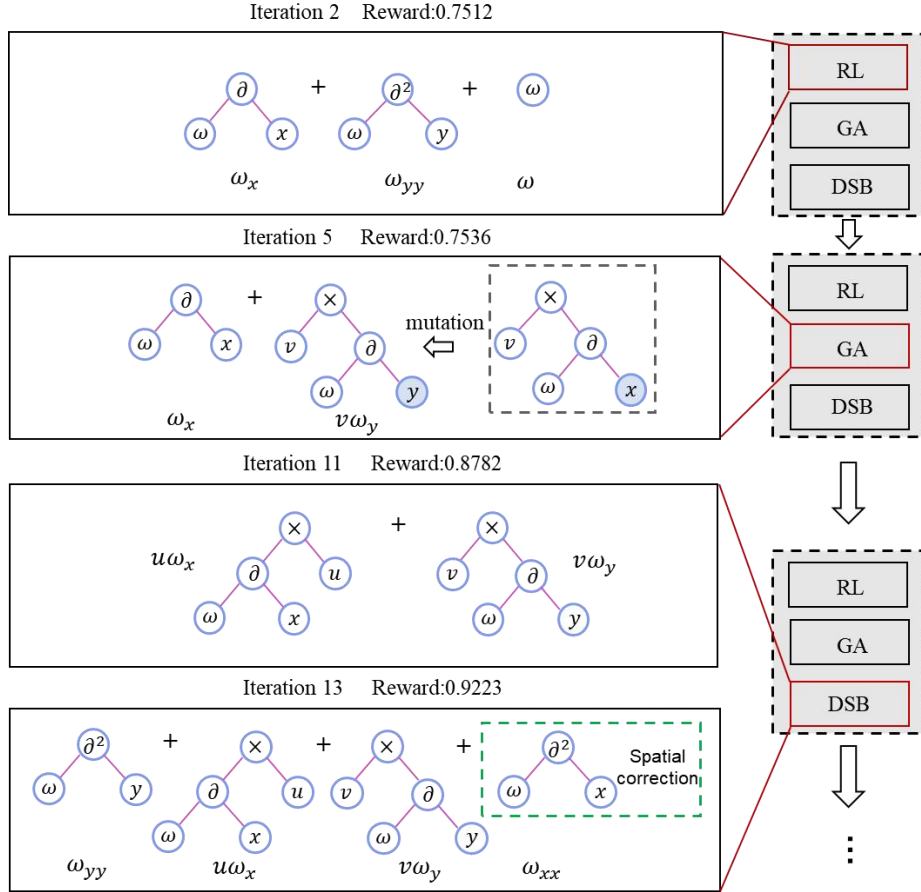


Fig. 9 Evolution of discovering NS equation.

Fig. 8 further illustrates the evolution of function terms during the optimization process and highlights the significance of a hybrid PDE generator, where RL generates expressions as initial samples, GA increases the stochasticity of the expressions, and DSB efficiently generates the final equations based on the possible combinations of the function terms. At the same time, spatial correction can further help to produce final physically correct equations. Table 7 demonstrates the performance of the framework to uncover the correct equations under different noise levels.

Table 7 Discovery of NS equation with the different noise levels.

Correct PDE: $\omega_t = 0.01\omega_{xx} + 0.01\omega_{yy} - u\omega_x - v\omega_y$			
Noise level	Identified PDE	Error (%)	L_2 error
10%	$\omega_t = 0.0094\omega_{xx} + 0.0094\omega_{yy} - 1.011u\omega_x - 0.994v\omega_y$	2.88	0.082
15%	$\omega_t = 0.0087\omega_{xx} + 0.0097\omega_{yy} - 0.987u\omega_x - 0.99v\omega_y$	3.93	0.083
25%	$\omega_t = 0.0084\omega_{xx} + 0.0097\omega_{yy} - 1.00u\omega_x - 0.982v\omega_y$	5.20	0.097

3.2.5 Discovering 3-D Gray–Scott reaction-diffusion model

Gray–Scott reaction–diffusion model is a two-component reaction-diffusion system, often used to model pattern formation and self-organization in a variety of scientific contexts [40,41]. The main difficulty in discovering this equation from data is that the dynamic system is governed by two PDEs and the available observations are both high-dimensional and of low resolution. This results in two key issues. First, the symbolic library, which is comprised of two state variables and four spatio-temporal variables, leads to an expansive search space and an increased susceptibility to local optimal solutions. Second, accurately solving the partial differentials becomes increasingly challenging with low-resolution data.

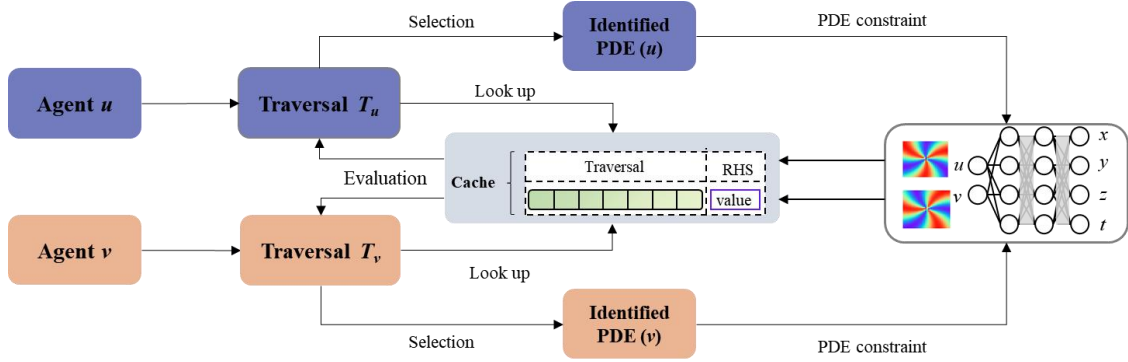


Fig. 10 Framework for discovering 3D Gray–Scott reaction–diffusion model.

To address these issues, we propose a modified discovering architecture, as depicted in Fig. 9. For each equation to be determined, different agents are employed to generate the corresponding PDE traversal. Since the primary time bottleneck lies in the evaluation of the generated traversal — specifically, the computation of the RHS of the equation, we adopt a caching mechanism. An extensible dictionary is constructed to record the traversal and its corresponding RHS value. This approach mitigates the need to repeat computations for generated traversals, thereby enhancing computation efficiency.

For the derivative evaluation, we use a PDE-constrained neural network to generate more metadata to avoid the problem of inaccurate prediction caused by low-resolution data. With 20% noise and 20% measurements of the total data volume, our framework is still able to find the final accurate equation with a 2.96% relative coefficient error, and the results are shown below:

$$\begin{cases} u_t = 0.019u_{xx} + 0.020u_{yy} + 0.018u_{zz} - 0.975uv^2 - 0.019u + 0.014 \\ v_t = 0.010v_{xx} + 0.010v_{yy} + 0.009v_{zz} + 1.020uv^2 - 0.069v \end{cases} \quad (21)$$

3.3 Comparison with other related methods

Embedding the uncovered physical equation into the predictive model (DNN) can significantly enhance the robustness of our framework to both limited and noisy data. The same idea has been applied to other methods, among which the more effective and influential methods mainly include DeepMod [23] and PINN-SR [24]. Both methods construct a compact candidate

library using prior knowledge, and add the residuals of the linear combinations of all the function terms and the left-hand side (LHS) of the equation u_t as a constraint into the training process of the neural network. L_1 regularization is also incorporated to ensure sparsity. The difference mainly lies in the determination of the final parsimonious PDE representation. The former achieves this by normalizing the function terms in the library and using the statistical properties of coefficients as the hard threshold to filter out trivial terms with small coefficients. PINN-SR, on the other hand, adopts an ADO strategy between DNN training and the STRidge method. We compare the performance of those two methods with our proposed framework on Burgers' equation, nonlinear Fisher-KPP equation, and KS equation. To enable a fair comparison, both DeepMod and PINN-SR were configured with basis function libraries of identical size, carefully incorporating all terms associated with the target equations. Related hyperparameters were kept consistent with those specified in the originating article and not adjusted under different noise levels. The corresponding code was taken from the GitHub repository provided in the paper¹.

Table 8 Comparison of different PDE discovery methods. Two levels of noise are considered. Low noise refers to 0.1, 0.1, 0.1, and high noise refers to 0.5, 0.3, 0.3 for those three datasets. There are three types of failure. Fail (1) is all of the true equation terms discovered with redundance; Fail (2) is part of the true equation terms identified without redundance; and Fail (3) is a much worse kind of result, which not only is the correct terms not found, but also contains the wrong terms.

PDE	Observations	Method	Error (E) (low noise)	Error (E) (high noise)
Burgers' equation	1000 (3.9%)	Our method	$0.86 \pm 0.93\%$	$2.28 \pm 0.82\%$
		DeepMod	$2.55 \pm 0.13\%$	Fail (1)
		PINN-SR	$0.88 \pm 0.03\%$	Fail (2)
Nonlinear Fisher-KPP equation	5000 (25%)	Our method	$1.13 \pm 0.084\%$	$14.12 \pm 14.31\%$
		DeepMod	Fail (3)	Fail (3)
		PINN-SR	Fail (3)	Fail (3)
KS equation	20583 (20%)	Our method	$1.15 \pm 1.86\%$	$9.46 \pm 10.21\%$
		DeepMod	$1.83 \pm 1.17\%$	Fail (3)
		PINN-SR	Fail (1)	Fail (3)

Table 8 demonstrates that our framework can successfully uncover the correct PDE in both high-level noise and low-level noise cases. The PINN-SR, which is sensitive to the hyperparameters of the sparsity penalty, tends to lack generalizability for equations without prior knowledge or with highly noisy data. DeepMod is also limited by the threshold setting and struggles to establish correct functional terms for equations with high variance in coefficients, such as the nonlinear Fisher-KPP equation. Note that both methods exhibit poor performance in this equation, and another potential reason for this lies in the construction of the overcomplete function term library. To enable the discovery of $(u_x)^2$, we introduce additional function terms $(\partial_x^m u)^2$ and their polynomial combinations with other terms into the library. It significantly increases the difficulty of training and escalates the training cost. The specific equations discovered by the three methods are provided in the Supplementary material. Fig. 10 further offers

¹ PINN-SR at <https://github.com/isds-neu/EQDiscovery> and DeepMod at https://github.com/PhIMaL/DecPyMoD_torch.

a comprehensive comparison of the performance of our method with DeepMod across different noise levels, including metrics such as L_2 , TPR, and E_2 . PINN-SR is not considered here since its performance is awful when more than 10% noise added. The comparison underscores that, even in the absence of prior knowledge, our method not only exhibits superior robustness to noisy data, but also boasts greater stability and general applicability.

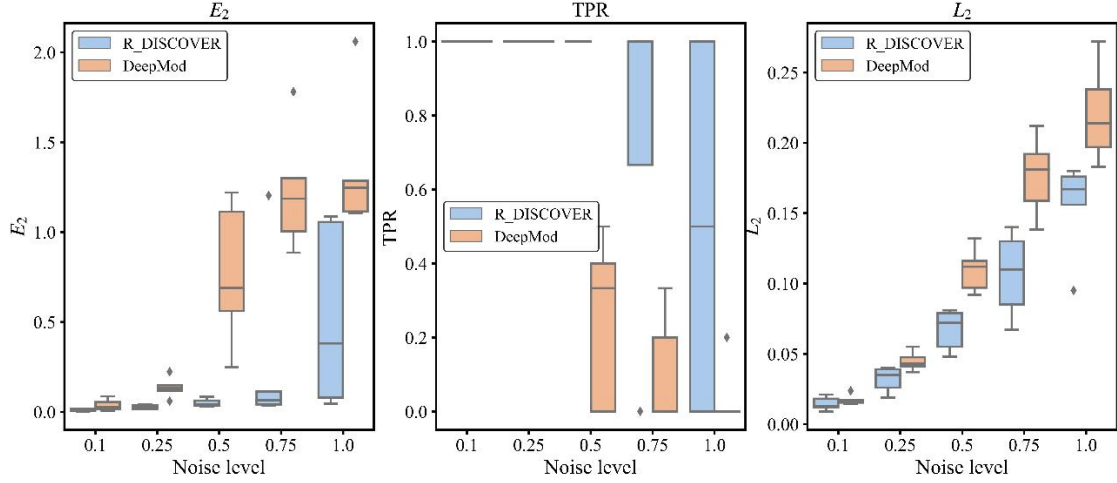


Fig. 11. Performance comparisons between our method with DeepMod on Burgers' equation. 1000 measurements are utilized and each experiment is repeated by 5 times with different random seeds.

3.4 Effect of stability selection

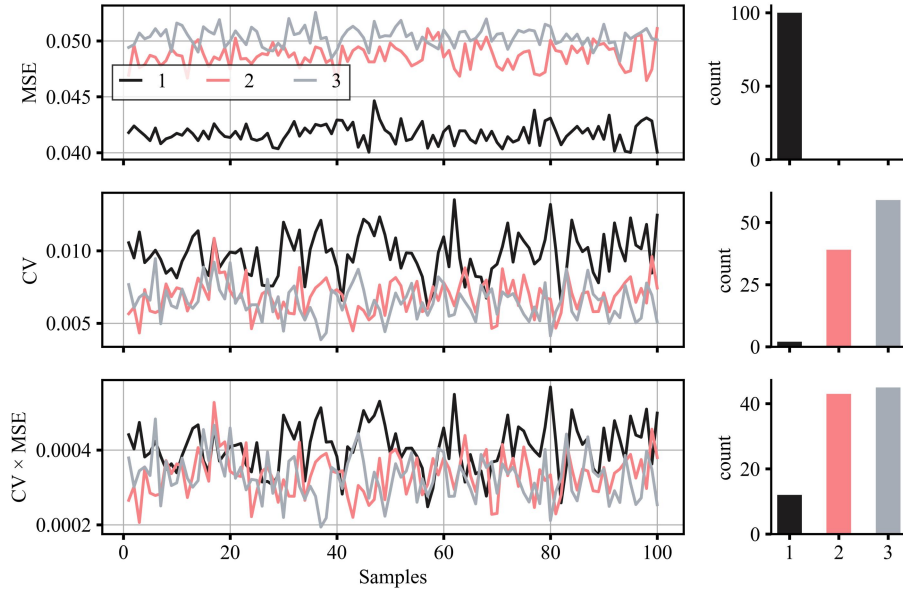


Fig. 12 Stability evaluation for classical Fisher-KPP equation.

At the end of the discovering process at each iteration, we keep the top K (default value is 3) expressions with the highest reward, and select the optimal samples based on the performance of the stability evaluation on the bootstrapped samples. The Fisher-KPP equations are taken as

examples for further illustration. As shown in Fig. 11, we provide the performance of the Top 3 expressions on different metrics. It can be seen that the residuals of the first expression are smaller in different subsets, i.e., they conform to the data better. Nevertheless, the coefficients of the function terms are more drastically varied, and therefore it ranks lower in the final ranking of $MSE \times CV$, which reveals that there may be an overfitting to the data. The specific statistics for the three expressions are shown in Table 9. For the nonlinear Fisher-KPP equation, expression 3 performs best in all three metrics, as shown in Fig. 12 and Table 10. It can be seen that the performance of discovering equations on full data is insufficient and can only partially reflect the fitness of data. Experiments show that further stability evaluation is necessary and their combinations can comprehensively evaluate the discovered PDE candidates and have better generalizability.

Table 9 Top 3 candidates for 1st round of searching classical Fisher-KPP equation.

Candidates (Top 3)	Identified PDE	Ranking
		$MSE \times CV$
1	$u_t = 0.023u_{xx} + 0.079u_x + 9.202u - 8.938u^2$	12
2	$u_t = 0.025uu_{xx} + 0.025(u_x)^2 + 7.548u - 7.147u^2$	43
3	$u_t = 0.023u_{xx} + 9.202u - 8.938u^2$	45

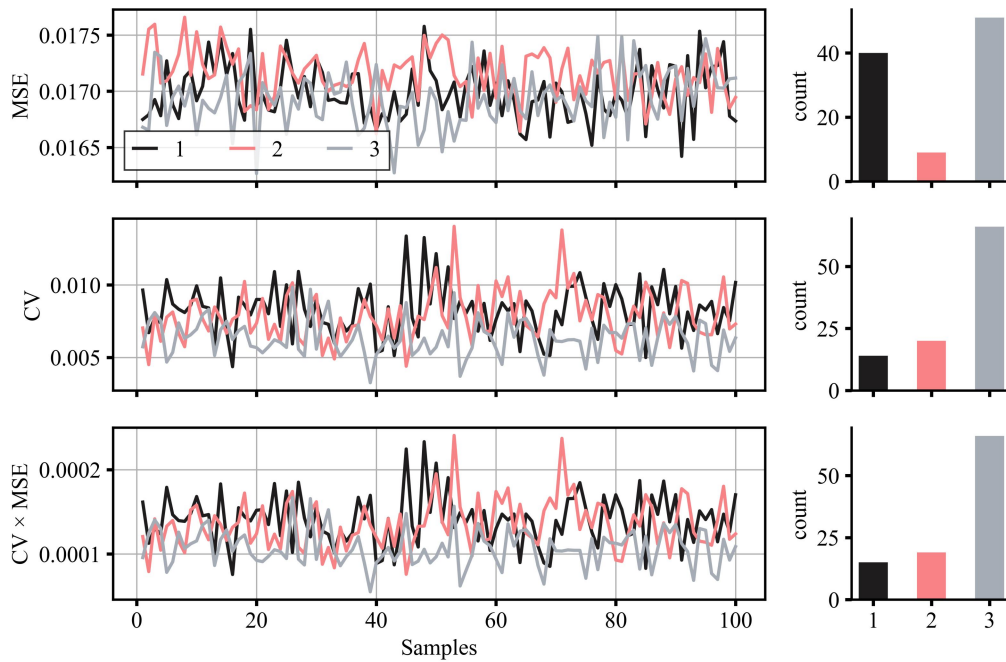


Fig. 13 Stability evaluation for Nonlinear Fisher-KPP equation.

Table 10 Top 3 candidates for 1st round of searching nonlinear Fisher-KPP equation.

Candidates (Top 3)	Identified PDE	Ranking
		$MSE \times CV$
1	$u_t = 0.011uu_{xx} + 0.011(u_x)^2 + 9.844u - 9.896u^2 - 0.001(u-x)^2$	15

2	$u_t = -0.06(u - x)^2 + 10.056u - 10.07u^2$	19
3	$u_t = 0.012u_{xx} + 0.012(u_x)^2 + 9.84u - 9.90u^2$	66

Conclusion

In this paper, we propose a framework named R-DISCOVER, which comprises two complementary and alternating update processes, including the discovering process and embedding process. During the discovering process, we discover open-form PDEs with a RL-guided hybrid PDE generator and automatically embed the PDE with the best performance as a physical constraint into DNN during the embedding process. We validated this framework on several numerical experiments, which demonstrates that it is capable of identifying the correct governing equations of complex and nonlinear dynamic systems from limited and highly noisy data. Compared with methods using an overcomplete candidate library, it offers superior flexibility and applicability since the dependence on prior knowledge is avoided with the symbolic representation. The novel hybrid PDE generator combines RL (neural guided), GA, and dynamic subtree bank, which enables the framework to generate diverse PDEs and handle lengthy and complex scenarios, such as Navier-Stokes equations, and Gray–Scott reaction-diffusion model. Notably, its robustness is further strengthened with a new stability metric incorporated, which shows greater universality compared with common sparsity-promoting methods relying on finetuning of hyperparameters. In the process of discovering the governing equations, our framework accomplishes the data interpretation and the construction of the prediction model simultaneously, which shows great potential for exploring real-world systems with limited understanding, which will be our future research. In addition, some efforts can be further made to better serve practical systems. Dealing with complex multi-dimensional systems requires a significant investment in training costs for the predictive model due to the vast amount of data involved. Additionally, the expression ability of DNN may be limited, necessitating the exploration of other network structures that are more powerful in expressive capacity. For example, convolutional neural networks could be employed to capture spatiotemporal features, which requires further comprehensive investigation.

Acknowledgments

This work was supported and partially funded by the National Center for Applied Mathematics Shenzhen (NCAMS), the Shenzhen Key Laboratory of Natural Gas Hydrates (Grant No. ZDSYS20200421111201738), the SUSTech – Qingdao New Energy Technology Research Institute, and the National Natural Science Foundation of China (Grant No. 62106116).

References

- [1] S.L. Brunton, J.L. Proctor, J.N. Kutz, Discovering governing equations from data by sparse identification of nonlinear dynamical systems, *Proc. Natl. Acad. Sci.* 113 (2016) 3932–3937.

- [2] S.H. Rudy, S.L. Brunton, J.L. Proctor, J.N. Kutz, Data-driven discovery of partial differential equations, *Sci. Adv.* 3 (2017) e1602614.
- [3] S. Sahoo, C. Lampert, G. Martius, Learning Equations for Extrapolation and Control, in: *Proc. 35th Int. Conf. Mach. Learn.*, PMLR, 2018: pp. 4442–4450.
- [4] Z. Long, Y. Lu, B. Dong, PDE-Net 2.0: Learning PDEs from data with a numeric-symbolic hybrid deep network, *J. Comput. Phys.* 399 (2019) 108925. <https://doi.org/10.1016/j.jcp.2019.108925>.
- [5] H. Xu, H. Chang, D. Zhang, DLGA-PDE: Discovery of PDEs with incomplete candidate library via combination of deep learning and genetic algorithm, *J. Comput. Phys.* 418 (2020) 109584. <https://doi.org/10.1016/j.jcp.2020.109584>.
- [6] M. Maslyaev, A. Hvatov, A.V. Kalyuzhnaya, Partial differential equations discovery with EPDE framework: Application for real and synthetic data, *J. Comput. Sci.* 53 (2021) 101345. <https://doi.org/10.1016/j.jocs.2021.101345>.
- [7] M. Schmidt, H. Lipson, Distilling Free-Form Natural Laws from Experimental Data, *Science.* 324 (2009) 81–85. <https://doi.org/10.1126/science.1165893>.
- [8] J. Bongard, H. Lipson, Automated reverse engineering of nonlinear dynamical systems, *Proc. Natl. Acad. Sci.* 104 (2007) 9943–9948. <https://doi.org/10.1073/pnas.0609476104>.
- [9] Y. Chen, Y. Luo, Q. Liu, H. Xu, D. Zhang, Symbolic genetic algorithm for discovering open-form partial differential equations (SGA-PDE), *Phys. Rev. Res.* 4 (2022) 023174. <https://doi.org/10.1103/PhysRevResearch.4.023174>.
- [10] M. Du, Y. Chen, D. Zhang, DISCOVER: Deep identification of symbolically concise open-form PDEs via enhanced reinforcement-learning, *arXiv preprint arXiv:2210.02181*, 2022.
- [11] M. Tang, W. Liao, R. Kuske, S.H. Kang, WeakIdent: Weak formulation for identifying differential equation using narrow-fit and trimming, *J. Comput. Phys.* 483 (2023) 112069. <https://doi.org/10.1016/j.jcp.2023.112069>.
- [12] D.A. Messenger, D.M. Bortz, Weak SINDy for partial differential equations, *J. Comput. Phys.* 443 (2021) 110525. <https://doi.org/10.1016/j.jcp.2021.110525>.
- [13] D.A. Messenger, D. Messenger, Online Weak-form Sparse Identification of Partial Differential Equations, *arXiv preprint arXiv:2203.03979*, 2022.
- [14] C. Bonneville, C. Earls, Bayesian deep learning for partial differential equation parameter discovery with sparse and noisy data, *J. Comput. Phys. X.* 16 (2022) 100115.
- [15] S.M. Hirsh, D.A. Barajas-Solano, J.N. Kutz, Sparsifying priors for Bayesian uncertainty quantification in model discovery, *R. Soc. Open Sci.* 9 (2022) 211823. <https://doi.org/10.1098/rsos.211823>.
- [16] S. Kim, P.Y. Lu, C. Loh, J. Smith, J. Snoek, M. Soljačić, Deep Learning for Bayesian Optimization of Scientific Problems with High-Dimensional Structure, *arXiv preprint arXiv:2104.11667*, 2022.
- [17] Z. Zhang, Y. Liu, Parsimony-enhanced sparse Bayesian learning for robust discovery of partial differential equations, *Mech. Syst. Signal Process.* 171 (2022) 108833.
- [18] H. Xu, DL-PDE: Deep-Learning Based Data-Driven Discovery of Partial Differential Equations from Discrete and Noisy Data, *Commun. Comput. Phys.* 29 (2021) 698–728. <https://doi.org/10.4208/cicp.OA-2020-0142>.

- [19] H. Schaeffer, Learning partial differential equations via data discovery and sparse optimization, *Proc. R. Soc. Math. Phys. Eng. Sci.* 473 (2017) 20160446.
- [20] M. Raissi, Deep hidden physics models: Deep learning of nonlinear partial differential equations, *J. Mach. Learn. Res.* 19 (2018) 932–955.
- [21] M. Raissi, P. Perdikaris, G.E. Karniadakis, Physics-informed neural networks: A deep learning framework for solving forward and inverse problems involving nonlinear partial differential equations, *J. Comput. Phys.* 378 (2019) 686–707.
- [22] G.E. Karniadakis, I.G. Kevrekidis, L. Lu, P. Perdikaris, S. Wang, L. Yang, Physics-informed machine learning, *Nat. Rev. Phys.* 3 (2021) 422–440. <https://doi.org/10.1038/s42254-021-00314-5>.
- [23] G.-J. Both, S. Choudhury, P. Sens, R. Kusters, DeepMoD: Deep learning for model discovery in noisy data, *J. Comput. Phys.* 428 (2021) 109985. <https://doi.org/10.1016/j.jcp.2020.109985>.
- [24] Z. Chen, Y. Liu, H. Sun, Physics-informed learning of governing equations from scarce data, *Nat. Commun.* 12 (2021) 6136. <https://doi.org/10.1038/s41467-021-26434-1>.
- [25] R. Stephany, C. Earls, PDE-READ: Human-readable partial differential equation discovery using deep learning, *Neural Netw.* 154 (2022) 360–382. <https://doi.org/10.1016/j.neunet.2022.07.008>.
- [26] P. Thanasutives, T. Morita, M. Numao, K. Fukui, Noise-aware physics-informed machine learning for robust PDE discovery, *Mach. Learn. Sci. Technol.* 4 (2023) 015009. <https://doi.org/10.1088/2632-2153/acb1f0>.
- [27] B.K. Petersen, M.L. Larma, T.N. Mundhenk, C.P. Santiago, S.K. Kim, J.T. Kim, Deep symbolic regression: Recovering mathematical expressions from data via risk-seeking policy gradients, in: *International Conference on Learning Representations*, 2020.
- [28] W. Tenachi, R. Ibata, F.I. Diakogiannis, Deep symbolic regression for physics guided by units constraints: toward the automated discovery of physical laws, *arXiv preprint arXiv:2303.03192*, 2023.
- [29] U. Fasel, J.N. Kutz, B.W. Brunton, S.L. Brunton, Ensemble-SINDy: Robust sparse model discovery in the low-data, high-noise limit, with active learning and control, *Proc. R. Soc. Math. Phys. Eng. Sci.* 478 (2022) 20210904. <https://doi.org/10.1098/rspa.2021.0904>.
- [30] H. Xu, J. Zeng, D. Zhang, Discovery of partial differential equations from highly noisy and sparse data with physics-informed information criterion, *Research.* 6 (2023) 0147.
- [31] F. Lejarza, M. Baldea, Data-driven discovery of the governing equations of dynamical systems via moving horizon optimization, *Sci. Rep.* 12 (2022) 11836. <https://doi.org/10.1038/s41598-022-13644-w>.
- [32] S. Cuomo, V.S. Di Cola, F. Giampaolo, G. Rozza, M. Raissi, F. Piccialli, Scientific machine learning through physics-informed neural networks: Where we are and what’s next, *J. Sci. Comput.* 92 (2022) 88.
- [33] J. Bec, K. Khanin, Burgers turbulence, *Phys. Rep.* 447 (2007) 1–66.
- [34] B. Saka, İ. Dağ, A numerical study of the Burgers’ equation, *J. Frankl. Inst.* 345 (2008) 328–348.
- [35] Z.-C. Wang, Z.-H. Bu, Nonplanar traveling fronts in reaction–diffusion equations with combustion and degenerate Fisher-KPP nonlinearities, *J. Differ. Equ.* 260 (2016) 6405–6450.

- [36] X. Tian, S. Guo, Traveling wave solutions for nonlocal dispersal Fisher–KPP model with age structure, *Appl. Math. Lett.* 123 (2022) 107593.
- [37] B. Contri, Fisher-KPP equations and applications to a model in medical sciences, (2016).
- [38] A.J. Chorin, Numerical solution of the Navier-Stokes equations, *Math. Comput.* 22 (1968) 745–762.
- [39] R. Mikulevicius, B.L. Rozovskii, Stochastic Navier–Stokes equations for turbulent flows, *SIAM J. Math. Anal.* 35 (2004) 1250–1310.
- [40] Y.N. Kyrychko, K.B. Blyuss, S.J. Hogan, E. Schöll, Control of spatiotemporal patterns in the Gray–Scott model, *Chaos Interdiscip. J. Nonlinear Sci.* 19 (2009).
- [41] J.S. McGough, K. Riley, Pattern formation in the Gray–Scott model, *Nonlinear Anal. Real World Appl.* 5 (2004) 105–121.

Supplementary Material for

Physics-constrained robust learning of open-form PDEs

from limited and noisy data

Mengge Du^a, Longfeng Nie^b, Siyu Lou^{c,d}, Yuntian Chen^{c,e,*}, Dongxiao Zhang^{c,f,*}

^a*College of Engineering, Peking University, Beijing, 100871, P.R. China*

^b*School of Environmental Science and Engineering, Southern University of Science and Technology, Shenzhen 518055, P. R. China*

^c*Eastern Institute for Advanced Study, Eastern Institute of Technology, Ningbo, 315200, Zhejiang, P.R. China*

^d*Department of Computer Science and Engineering, Shanghai Jiao Tong University, 200240, Shanghai, P.R.China*

^e*Ningbo Institute of Digital Twin, Eastern Institute of Technology, Ningbo, 315200, Zhejiang, P.R. China*

^f*National Center for Applied Mathematics Shenzhen (NCAMS), Southern University of Science and Technology, Shenzhen, 518000, Guangdong, P. R. China*

*Corresponding author

Email address: ychen@eias.ac.cn, zhangdx@sustech.edu.cn.

1. Experimental settings

We conducted all the experiments with an NVIDIA A100 GPU card. The detailed hyperparameter setting in R-DISCOVER is provided in Table 1.

Table 1 Hyperparameters

Hyperparameter	Default value	Definition
N_s	100	Number of bootstrapped subsets
N_p	10	Number of subsamples for calculating the coefficients of variation
N_{sub}	10	The size of the basis function library subsampled from DSB
λ_1	0.1	Coefficients of physics loss term on collocation points
λ_2	0	Coefficients of physics loss term on refined collocation points
d_{max}	4	Maximum depth of subtrees
ζ_1	0.01	Penalty coefficients of the number of function terms
ζ_2	0.0001	Penalty coefficients of the maximum depth of subtrees
ε	0.02	Threshold of reserved expressions
p_{cross}	0.8	Probability of conducting the crossover operation
p_{mut}	0.5	Probability of conducting the mutation operation

2. Reconstructed field with a predictive model trained with discovered equation

Our method can not only find the underlying governing equation from the noisy data, but also construct a prediction model for the nonlinear system response. With the discovered equation incorporated, it can provide more accurate predictions. The reconstructed fields predicted by the DNN for different systems are shown below.

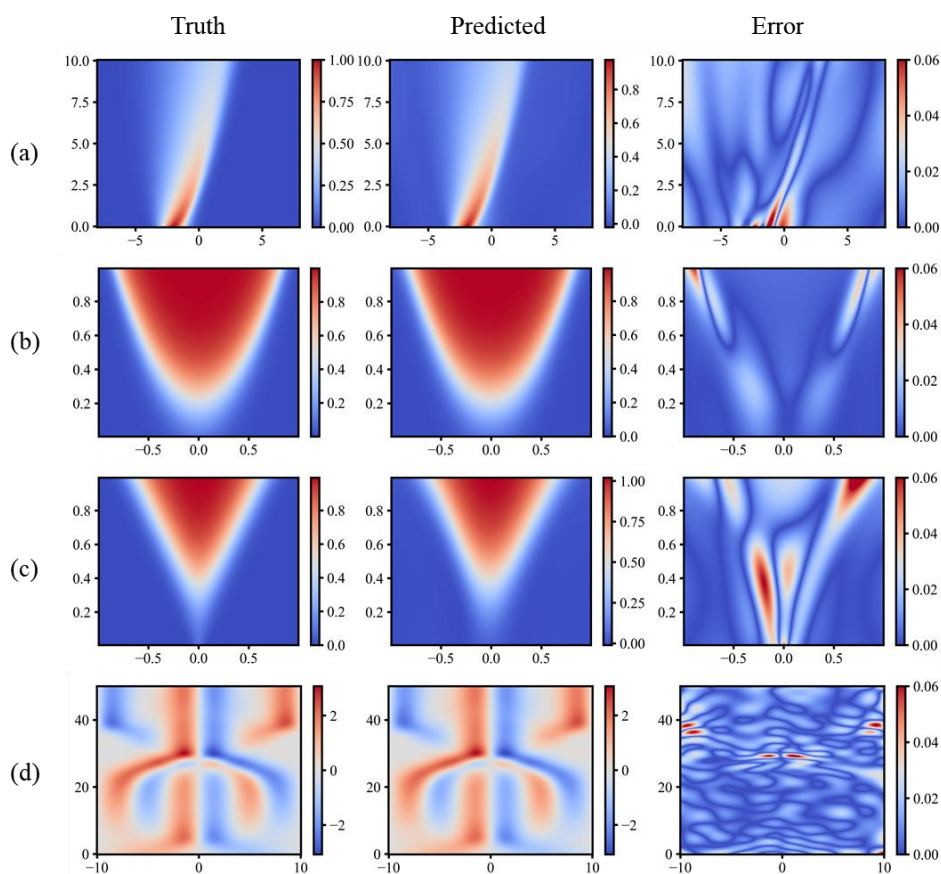


Fig. 1 Predicted solutions for (a) Burgers' equation with 100% noise and 1000 data points; (b) classical Fisher-KPP with 100% noise and 5000 data points; and (c) nonlinear Fisher-KPP equation with 50% noise and 10000 data points; (d) KS equation with 15% noise and 26214 data points.

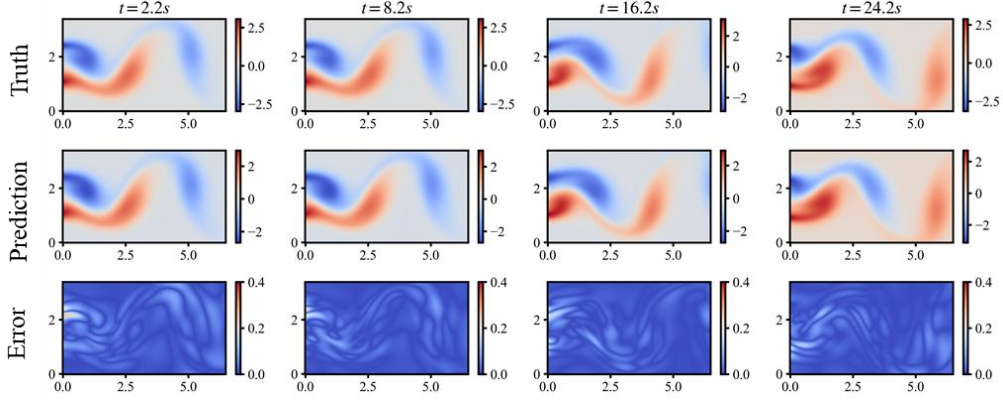


Fig. 2 Predicted solutions for Navier-Stokes equation at different time steps with 25% noise and of total measurements.

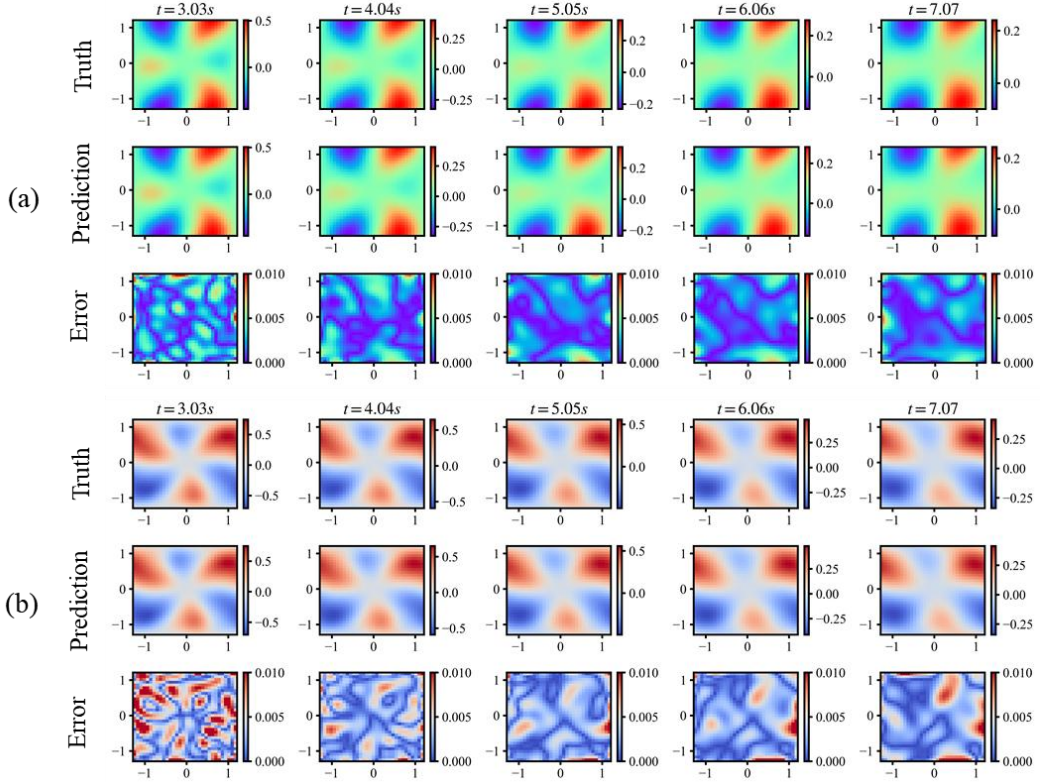


Fig. 3 Predicted solutions for a 3D reaction-diffusion model of (a) u and (b) v at different time steps with 20% noise and 20% of total measurements.

3. Comparison with PINN-based method

We compared the performance of our model with two PINN-based methods, including PINN-SR [1] and DeepMod [2] at three nonlinear governing equations. The concrete discovered equations under different levels of noise are shown in Table 2.

Table 2 The discovered equation by our framework and other related method

PDE	Noise level	Method	Discovered equation
Burgers'	10%	Our method	$u_t = 0.0985u_{xx} - 0.998uu_x$

equation	DeepMod	$u_t = 0.095u_{xx} - 1.004uu_x$
	PINN-SR	$u_t = 0.099u_{xx} - 0.986uu_x$
	Our method	$u_t = 0.102u_{xx} - 1.029uu_x$
50%	DeepMod	$u_t = 0.066u_{xx} - 0.521uu_x + 0.1376uu_{xx} + 0.2637u^2$
	PINN-SR	$u_t = -0.081u_x$
	Our method	$u_t = 0.0196uu_{xx} + 0.0196u_x^2 + 10.029u - 10.024u^2$
10%	DeepMod	$u_t = 0.634u_x^2 - 0.118uu_{xxx} + 0.224u^2u_{xxx} - 0.124u^3u_{xxx}$
	PINN-SR	$u_t = 5.657u - 5.787u^3$
Nonlinear Fisher-KP P equation	Our method	$u_t = 0.015uu_{xx} + 0.015u_x^2 + 9.894u - 9.859u^2$
30%	DeepMod	$u_t = 0.588u_x^2 + 2.967u - 0.106uu_{xxx} + 0.208u^2u_{xxx} - 0.120u^3u_{xxx}$
	PINN-SR	$u_t = 5.821u - 5.901u^3$
10%	Our method	$u_t = -0.982uu_x - 0.984u_{xx} - 0.988u_{xxxx}$
	DeepMod	$u_t = -1.015uu_x - 0.980u_{xx} - 0.992u_{xxxx}$
	PINN-SR	$u_t = -1.015uu_x - 1.00u_{xx} - 0.993u_{xxxx} + 7 \text{ redundant terms}$
KS equation	Our method	$u_t = -0.941uu_x - 0.885u_{xx} - 0.879u_{xxxx}$
30%	DeepMod	$u_t = -1.189uu_x - 1.0951u_{xx} - 1.0760u_{xxxx} + 0.236u^2u_{xx} + 0.183u^2u_{xx}$

References

- [1] Z. Chen, Y. Liu, H. Sun, Physics-informed learning of governing equations from scarce data, Nat. Commun. 12 (2021) 6136. <https://doi.org/10.1038/s41467-021-26434-1>.
- [2] G.-J. Both, S. Choudhury, P. Sens, R. Kusters, DeepMoD: Deep learning for model discovery in noisy data, J. Comput. Phys. 428 (2021) 109985. <https://doi.org/10.1016/j.jcp.2020.109985>.